Instabilities of the normal state in current-biased narrow superconducting strips

Yury N. Ovchinnikov,[1,2] Andrey A. Varlamov,[3] Gregory J. Kimmel,[4] and Andreas Glatz[4,5]
[1]*Landau Institute for Theoretical Physics, RAS, Chernogolovka, Moscow District 142432, Russia*
[2]*Max-Plank Institute for Physics of Complex Systems, 01187 Dresden, Germany*
[3]*Istituto Superconduttori, Materiali Innovativi e Dispositivi (CNR-SPIN), Viale del Politecnico 1, 00133 Rome, Italy*
[4]*Materials Science Division, Argonne National Laboratory, 9700 S Cass Avenue, Lemont, Illinois 60439, USA*
[5]*Department of Physics, Northern Illinois University, DeKalb, Illinois 60115, USA*

(Received 3 May 2019; revised manuscript received 5 November 2019; published 24 January 2020)

We study the current-voltage characteristic of narrow superconducting strips in the gapless regime near the critical temperature in the framework of the Ginzburg-Landau model. Our focus is on its instabilities occurring at high current biases. The latter are consequences of dynamical states with periodic phase-slip events in space and time. We analyze their structure and derive the value of the reentrance current at the onset of the instability of the normal state. It is expressed in terms of the kinetic coefficient of the time-dependent Ginzburg-Landau equation and calculated numerically.

DOI: 10.1103/PhysRevB.101.014511

I. INTRODUCTION

Narrow superconducting strips are the subject of great interest for superconducting quantum electronic devices. Their dissipationless state is very subtle and sensitive to thermal and quantum fluctuations, which can easily flip the superconducting strip into the resistive state, making them ideal candidates for very sensitive detectors. Various models have been proposed to explain the appearance of nonzero resistance in these strips and its temperature dependence in the region of low temperatures (for a review, see Refs. [1,2]).

The role of thermal fluctuations responsible for energy dissipation, when current flows through a one-dimensional superconductor, was considered for the first time in the seminal paper by Langer and Ambegaokar [3] over 50 years ago. Note that a realistic "one-dimensional superconductor" is, in fact, a narrow strip with finite width W, much less than the Ginzburg-Landau coherence length $\xi(\tau) \propto (k_B T_c \tau)^{-1/2}$, where $\tau = 1 - T/T_c$ is the reduced temperature and T_c is the critical temperature. The solution of the Ginzburg-Landau equation for a superconducting wire with applied current j shows that a homogeneous superconducting state, i.e., a finite, but current-dependent, global order parameter, exists up to a certain critical current $j_c = 0.0312(W/\xi) j_{dp}$, where j_{dp} is the depairing current at which superconductivity is completely suppressed. For currents $j_c < j < j_{dp}$ thin superconducting wires [4–12] or superfluids [13–15] are in the resistive state, where the mechanism for dissipation is related to phase-slip processes, i.e., the processes of vortices/flux quanta crossing the strip [16]. These phase-slip events occur randomly [17]. If j is even larger than j_{dp}, the system is in the normal state, but fluctuating local superconducting regions can temporally appear.

In contrast to the case of increasing current, which destroys superconductivity, here we are investigating the situation when the applied current is initially so large that the superconducting strip is in the normal state despite the temperature being below the critical temperature. Starting from this initial state, the current j in the narrow superconducting strip is then lowered, such that superconductivity is reestablished in the system. Our goal is to study the corresponding current-voltage (I-V) characteristics. In particular, we derive the value of the reentrance current density j_r at the onset of the instability of the normal state when the applied current decreases. Our consideration is valid in the gapless region at temperatures slightly below the critical one, where the time-dependent Ginzburg-Landau equation holds.

It is important to note that the considered situation is quite different from the problem of determining the critical current at which the superconductor becomes normal (see Refs. [18,19]). The authors of the cited papers, which are based on the works by Gorkov [20] and Kulik [21], also remark that the normal state remains stable for any finite value of E when the applied current is lowered from the normal state. However, the linear analysis used to study the instability of the superconducting state is not suitable for analyzing the instability of the normal state. In the latter case higher-order stability analysis is required, which we address in this paper. An important result we obtained is that the exponential growth of superconducting fluctuations in a time interval determined by $j\Delta t < \hbar\sigma/[e\xi(\tau)]$ (σ is the normal conductivity) leads to an instability of the normal state, which cannot be derived from linear perturbation theory as fluctuations are captured only beyond this mean-field approach. As a consequence, the system enters a dynamical superconducting state at some finite electric field. We will show below that there is a series of the electric field values for which the normal state starts to become unstable even for infinitely small perturbations.

In the following we describe the model and show the analysis of the time-dependent Ginzburg-Landau equation near the critical point of the normal state. We derive the value of the reentrance current and order parameter values by expanding the current up to second order in the electric field at the critical points. Details of the calculations can be found in the Appendixes. We start with introducing the model in the following section and then analyze the I-V characteristics close to the depairing current and near the instability points of the normal state.

II. MODEL

In this paper we approximate the narrow superconducting strip of width W smaller than the superconducting coherence length by a one-dimensional (1D) system, described by the time-dependent Ginzburg-Landau equation (TDGLE). The TDGLE can be written in dimensionless variables, without accounting for thermal fluctuations and magnetic field (the latter does not appear in the 1D model) in the form

$$\mathfrak{u}(\partial_t + i\mu)\psi = \partial_x^2\psi + (1 - |\psi|^2)\psi, \tag{1}$$

where ψ is the complex order parameter and μ is the scalar potential. The reduced relaxation rate $\mathfrak{u}$ controls the system's evolution in time and is given by

$$\mathfrak{u} = \mathfrak{u}_0 \frac{\pi^4}{14\zeta(3)} \frac{e^2\nu\mathfrak{D}}{\sigma}, \tag{2}$$

where ν is the density of states at the Fermi surface, $\mathfrak{D}$ is the effective diffusion constant, ζ is the Riemann zeta function, and $\mathfrak{u}_0$ is a numerical constant [22,23].

The fixed total bias current consists of the sum of normal (j_n) and superconducting (j_s) components and in turn can be related to the space derivatives of the complex order parameter and the scalar potential:

$$j = j_n + j_s = -\partial_x\mu - \mathrm{Im}(\psi^*\partial_x\psi). \tag{3}$$

Time and distance in Eqs. (1)–(3) are measured in units of $t_0 = 8\pi\sigma\lambda^2/c^2$ and scaled superconducting coherence length, $\xi = (\frac{\pi\mathfrak{D}}{16k_BT_c\tau})^{1/2}$, respectively, with λ being the London penetration depth. The electrical current density j is measured in units of $j_0 = c\Phi_0/(8\pi^2\lambda^2\xi\sqrt{2})$ (Φ_0 is the flux quantum). In these units the depairing current density reads $j_{dp} = 2/(3\sqrt{3})j_0 \approx 0.385j_0$.

In what follows, it is useful to transform the scalar potential to the form

$$\mu = -Ex + \tilde{\mu}, \tag{4}$$

where E is the average electric field, which is equal to the average normal current in dimensionless units, and $\tilde{\mu}$ is the spatially and temporally fluctuating part of μ.

Phase-slip events generate instabilities in the current-voltage characteristics, which will be the main subject of this work. In particular, these processes cause strong changes in the electric field and order parameter at their space-time coordinates. We take their effect into account explicitly by introducing a corresponding effective electric potential $\tilde{\mu}$ to the TDGLE.

A phase-slip process in a strip of finite width is related to the transfer of a magnetic vortex-antivortex pair across it. Each such event is accompanied by the suppression of the order parameter and, consequently, of the supercurrent. Due to the conservation of the total current, a sharp peak in the normal current appears at the time and space location of the phase-slip event.

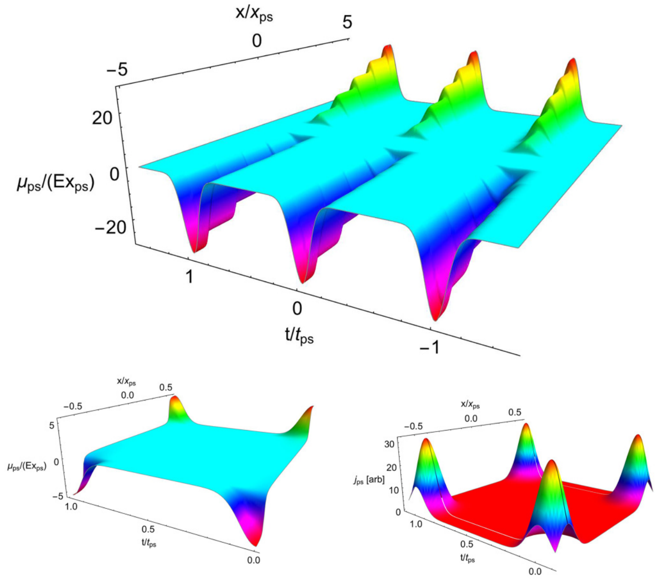

FIG. 1. Top: Illustration of phase-slip potential μ_{ps}, Eq. (6), as a function of time and space and finite-width δ functions (see text). Bottom: Close-up of region $\mathcal{A}_{ps}$ (left) and related j_{ps} (right) in the same region.

In the large-current regime, $j > j_{dp}$, superconductivity should be destroyed by the applied current according to the mean-field approximation, and the system is in the normal state with Ohmic I-V characteristics. Yet the proximity to the superconducting transition promotes superconducting fluctuations in the system, which in our case will be realized by (anti)"phase-slip" events (ps) which are periodic in time and space. In this regime some domains of the strip will temporally become superconducting. The corresponding periods in time and space are denoted as t_{ps} and x_{ps}, respectively. Outside a very narrow region in the time-space plane one can rewrite Eq. (1) in the form

$$\mathfrak{u}[\partial_t + \imath(\tilde{\mu} + \mu_{ps} - E\tilde{x})]\psi = \partial_x^2\psi + (1 - |\psi|^2)\psi. \tag{5}$$

Here $\tilde{x} = x \mod (x_{ps}/2)$, and the associated potential

$$\mu_{ps} = Ex_{ps}t_{ps}\sum_k \delta(t - t_{ps}k)\sum_m m\Theta \times \left[x - x_{ps}\left(m - \frac{1}{2}\right)\right]\Theta\left[x_{ps}\left(m + \frac{1}{2}\right) - x\right], \tag{6}$$

where the quantization condition $Ex_{ps}t_{ps} = 2\pi$ is implied. The shape of μ_{ps} is illustrated in Fig. 1 (top) with smoothed step and δ functions. In the bottom panels μ_{ps} and $j_{ps} \propto \partial_x\mu_{ps}$ are shown in the elementary space-time cell $\mathcal{A}_{ps} \equiv]-x_{ps}/2; x_{ps}/2[\times]0; t_{ps}[$. The latter illustrates the mentioned spikes in the normal current at the phase-slip event location.

These additional terms do not contribute to the electric field inside $\mathcal{A}_{ps}$, only at its corners. The solution for the order parameter ψ away from the corners of $\mathcal{A}_{ps}$ follows from Eq. (5) with periodic boundary conditions. The size of the region with strong suppression of ψ is of order $W \times Wt_{ps}/x_{ps}$, where W is the width of the strip.

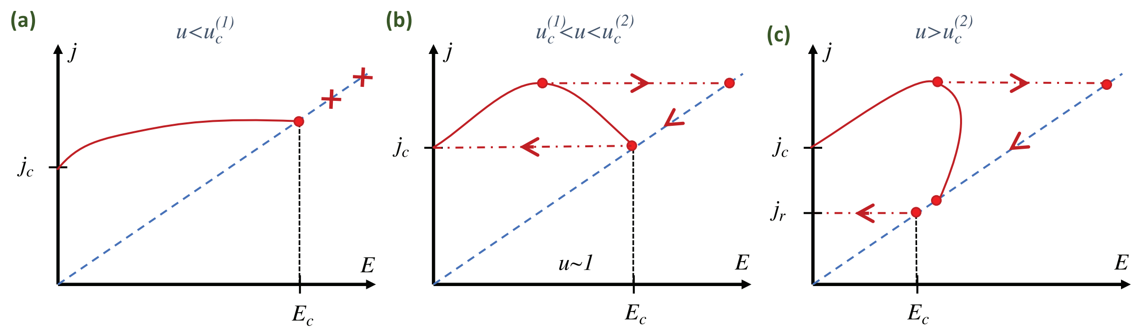

FIG. 2. Illustration of possible I-V (or I-E) curves for different $\mathfrak{u}$. (a) The case of a reversible, nonhysteretic situation for small $\mathfrak{u}$ below some value $\mathfrak{u}_c^{(1)}$. Actual "trajectories" are indicated by arrowheads and crosses. (b) Some intermediate-$\mathfrak{u}$ regime where the realized I-V hysteresis has a reentrance current equal to the critical current j_c. Note that the reentrance current cannot be larger than j_c since one would be required to overcome a threshold (see text). (c) Above a value $\mathfrak{u}_c^{(2)}$ the reentrance current is lower than the critical current j_c. The latter is the realized hysteresis curve.

III. ANALYSIS OF THE I-V CHARACTERISTICS

Let us start with the analysis of Eqs. (1)–(4). Within the unit cell $\mathcal{A}_{\text{ps}}$, one can write the Fourier ansatz for the complex order parameter

$$\psi = \sum_{k=-\infty}^{\infty} A_k e^{\imath Qkx}, \tag{7}$$

where Q should be found from the local minimum conditions of E for a given current density j.

Correspondingly, Eq. (3) acquires the form

$$j = E + Q\sum_k k|A_k|^2. \tag{8}$$

Plugging ansatz (7) into Eq. (1) gives

$$\begin{aligned}
&-\imath\mathfrak{u}\left\{Ex + \frac{\imath}{2}\sum_{k\neq 0} k^{-1}[A_1(2-k)A^*_{1-k} + A^*_1(2+k)A_{k+1}]e^{\imath kQx} - \frac{\imath}{2}\sum_{l\neq k\neq 1}\frac{k+l}{k-l}A^*_k A_l e^{-\imath(k-l)Qx}\right\}\sum_{k=-\infty}^{\infty} A_k e^{\imath kQx} \\
&= (1-|A_1|^2 - Q^2)A_1 e^{\imath Qx} + \sum_{k\neq 1}\Bigg\{(1-2|A_1|^2 - k^2Q^2)A_k e^{\imath kQx} - A_1^2 A_k^* e^{-\imath(k-2)Qx} \\
&\quad - \sum_{l\neq 1}\left[2A_1A_kA^*_l e^{\imath(k-l+1)Qx} + A^*_1A_kA_l e^{\imath(k+l-1)Qx} + \sum_{m\neq 1}A_kA_lA^*_m e^{\imath(k+l-m)Qx}\right]\Bigg\}.
\end{aligned} \tag{9}$$

Finally, accounting for the charge conservation condition $\text{div}\, j = 0$ and Eq. (3), one can find the expression for the fluctuating part of the scalar potential $\tilde{\mu}$ in terms of the introduced Fourier coefficients:

$$\tilde{\mu} = -\frac{\imath}{2}\left\{\sum_{k\neq 0}\frac{e^{\imath kQx}}{k}[A_1(2-k)A^*_{1-k} + A^*_1A_{k+1}(2+k)] - \sum_{k\neq l\neq 1}\left(\frac{k+l}{k-l}\right)e^{-\imath(k-l)Qx}A^*_kA_l\right\}. \tag{10}$$

In Eqs. (9) and (10) we explicitly separated the quantity A_1 since it is the dominant Fourier component in the vicinity of the critical point $j = j_{\text{dp}}$ and plays an important role throughout the paper. Fourier coefficients with $|k| \gg 1$ quickly decay. All other coefficients in this region can be found in the framework of perturbation theory.

Equation (9) enables us to obtain the I-V characteristics in the complete domain of dynamical resistive states. The above-mentioned minimization with respect to E allows us to finds the shape of the I-V characteristics, which turns out to be critically dependent on the value of the dynamic coefficient $\mathfrak{u}$ of the TDGLE.

One can expect to find three qualitatively different types of I-V characteristics, which are illustrated in Fig. 2. The first one [Fig. 2(a)] is reversible and could be realized when the dynamic coefficient $\mathfrak{u}$ is sufficiently small: $\mathfrak{u} < \mathfrak{u}_c^{(1)}$, where $\mathfrak{u}_c^{(1)}$ is the first critical value, which will be obtained below. In the case where $\mathfrak{u} > \mathfrak{u}_c^{(1)}$ the I-V characteristics become irreversible [Figs. 2(b) and 2(c)].

In the case of strong damping, when $\mathfrak{u}$ exceeds the second critical value $\mathfrak{u}_c^{(2)}$, the transition to a finite value of the order parameter happens at a smaller E_c value, which is where we define the *reentrance* current j_r. Calculation of the order parameter value in the vicinity of the critical point $(\mathfrak{u}E)_c$ (see below) shows that in practice only the latter scenario of the I-V characteristics, shown in Fig. 2(c), is realized.

A. Current density close to the depairing current

Next, we consider the case when the bias current density j is close to j_{dp}. Equation (1) allows us to obtain the above-mentioned value of j_{dp}, which destroys superconductivity in the 1D channel, where the corresponding critical value of the order parameter is $\psi_c = \sqrt{2/3}$, and the value of the wave vector (for $E = 0$) is $Q_c = 1/\sqrt{3}$. Close to this point, Eq. (9) is decomposed into two equations with $\{k, 2-k\}$. A detailed analysis of the Fourier coefficients and the determination of the wave vector Q is presented in Appendix A. As a result of these calculations we obtain the electric field dependence of the current density to second order, close to its depairing value, as

$$j = j_{\rm dp} + E - E^2\gamma(\mathfrak{u}), \quad (11)$$

where the calculation of the coefficient $\gamma(\mathfrak{u})$ of the quadratic term as a function of $\mathfrak{u}$ is a highly involved task but can be performed exactly for any value of $\mathfrak{u}$ and can be expressed as a full derivative:

$$\gamma(\mathfrak{u}) = -3\sqrt{3}\mathfrak{u}^2\frac{\partial}{\partial\mathfrak{u}}\left[\frac{\pi}{2\sqrt{2\mathfrak{u}}}\left\{\coth(\pi\sqrt{2\mathfrak{u}}) - \frac{1}{\pi\sqrt{2\mathfrak{u}}}\right\}\right.$$
$$\left.\times\left(1-\frac{6}{\mathfrak{u}}+\frac{12}{\mathfrak{u}^2}\right)+\frac{\pi^2}{\mathfrak{u}}\left(1-\frac{2}{\mathfrak{u}}\right)+\frac{4\pi^4}{15\mathfrak{u}}\right]. \quad (12)$$

The explicit expression of the full derivative is given in Appendix A, Eq. (A8), and $\mathcal{D}$ is defined there in Eqs. (A1b) and (A2). Note that the difference in braces behaves as $\pi\sqrt{2\mathfrak{u}}/3$ for small $\mathfrak{u}$, such that all terms $\propto\mathfrak{u}^{-2}$ under the derivative cancel, and the complete expression is nonsingular at $\mathfrak{u} = 0$. Therefore, in the limit of small $\mathfrak{u}$ we keep the first two terms of the sum in (12) and expand the remaining sum to first order. This gives

$$\gamma(\mathfrak{u}) = \frac{18}{\sqrt{3}}\mathfrak{u}^2\left(\frac{61}{(1+2\mathfrak{u})^2}+\frac{7}{(4+2\mathfrak{u})^2}\right.$$
$$\left.+0.0486531 - 0.0185438\mathfrak{u}\right). \quad (13)$$

For large values of $\mathfrak{u}$ ($\mathfrak{u} \gg 1$), we obtain from Eq. (12) (using the asymptotic expressions of the coth and $\sinh^{-2}$ terms)

$$\gamma(\mathfrak{u}) = \sqrt{3}\left(3\pi^2+\frac{4\pi^4}{5}-\frac{3}{4}+\frac{3\pi}{8}\sqrt{2\mathfrak{u}}\right)$$
$$-\frac{27\pi}{2}\sqrt{\frac{3}{2\mathfrak{u}}}-\frac{3[\sqrt{3}(4\pi^2-3)]}{\mathfrak{u}}$$
$$+\sqrt{\frac{3}{2}}\frac{45\pi}{\mathfrak{u}^{3/2}}-\frac{27\sqrt{3}}{\mathfrak{u}^2}+O(\mathfrak{u}e^{-2\pi\sqrt{2\mathfrak{u}}}). \quad (14)$$

The $\mathfrak{u}$ dependence of $\gamma(\mathfrak{u})$ and the domains of validity of its approximations (13)-(14) are presented in Fig. 3. $\mathfrak{u} \sim 1$ separates the regions where small-$\mathfrak{u}$ and large-$\mathfrak{u}$ approximations work best; that is, the relative deviations from the exact curve are both minimum at $\mathfrak{u} = 1.061$, less than 10^{-3}.

Note that in Eqs. (11), (12), and (A4) a free structural parameter Q is present. Its value can be estimated (in higher orders of the perturbation theory over E) from the condition that the mean value of the electric field in the strip should be extremal for each given value of the current.

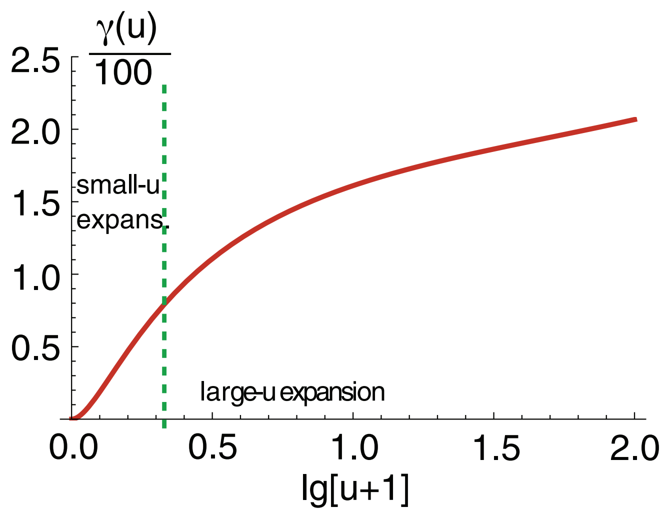

FIG. 3. Half-exponential plot of the coefficient $\gamma(\mathfrak{u})$ [Eq. (12)] of the E^2 term in our approximation for the current. Below $\mathfrak{u} \sim 1$ (vertical dashed line) the small-$\mathfrak{u}$ approximation [Eq. (13)] is indistinguishable from the exact curve, while for $\mathfrak{u} \gtrsim 1$ the large-$\mathfrak{u}$ expression [Eq. (14)] is indistinguishable from the exact one.

B. Vicinity of the critical points

We now consider the vicinity of critical points $(\mathfrak{u}E)_c$, which are defined by the condition

$$\frac{\partial(\mathfrak{u}E)}{\partial Q} = 0. \quad (15)$$

In this region we search for the solution to the nonlinear problem (9) by its linear expansion over eigenfunctions. Therefore, the linearized condition of Eq. (15) can be understood as the following eigenvalue problem:

$$\hat{L}\mathbf{f} = 0, \quad (16)$$

where the form of the linear operator $\hat{L}$ follows from Eq. (9):

$$\hat{L}_{k,l} = \begin{cases} Z_{k-1}\delta_{l,1} + Z_{k-l}(1-\delta_{l,1}) + (Q^2k^2-1)\delta_{k,l}, & k \neq 1, \\ Z_{1-l} - (1-Q^2)\delta_{l,1}, & k = 1, \end{cases} \quad (17)$$

with

$$Z_k = \begin{cases} \frac{\mathfrak{u}E}{kQ}(-1)^k, & k \neq 0, \\ 0, & k = 0. \end{cases} \quad (18)$$

The eigenvector $\mathbf{f}$ of Eq. (16) is related to the Fourier coefficients at the critical points in the following way:

$$\{f_k\} \leftrightarrow \{A_{k\geqslant 2}, A_1, A_{k\leqslant 0}\}, \quad (19)$$

where $f_1 \leftrightarrow A_1$.

The above eigenvalue problem has possibly an infinite number of solutions $\{(\mathfrak{u}E)_c, Q_c\}$. Note that the quantities $\mathfrak{u}$ and E appear in the form of a product only at the critical point [in contrast to Eqs. (11) and (12)]. The linearized equation can be solved numerically, and the eight largest critical points (defined by simultaneous eigenvalues of $\hat{L}$ and $\hat{L}^\dagger$) are listed in Table I (the corresponding normalized eigenvectors of $\hat{L}$ and $\hat{L}^\dagger$ (here $\hat{L}^\dagger = \hat{L}^{\mathsf{T}} \neq \hat{L}$) are given in the Supplemental Material [24]). Below we discuss the numerical solution in more detail.

TABLE I. The eight largest simultaneous eigenvalue pairs $\{(\text{u}E)_c, Q_c\}$ of $\hat{L}$ and $\hat{L}^\dagger$ for $N_k = 24$ Fourier components and corresponding solvability coefficients $\{\lambda_1, \lambda_2, \lambda_3\}$. Labels ν correspond to the intersection points shown in Fig. 4. The critical value $\nu = 3$ (bold) corresponds to the transition point to the superconducting state without a threshold - see text.

ν	$(\text{u}E)_c$	Q_c	λ_1	λ_2	λ_3
1	0.320	0.486	0.166	−0.503	−0.176
2	0.276	0.537	0.102	−0.230	−0.0787
3	**0.21**	**0.335**	**−0.0478**	**0.128**	**0.030**
4	0.189	0.359	0.0265	−0.0671	−0.0169
5	0.156	0.256	0.0133	−0.0345	−0.00570
6	0.144	0.27	0.0074	−0.0183	−0.00258
7	0.124	0.208	0.00348	−0.00922	−0.000833
8	0.116	0.217	0.00199	−0.00528	−0.000436

In order to get further insight into the behavior of the I-V characteristic near these critical points and to determine the type of instability point (first- or second-order transition), we introduce the operator $\delta\hat{L}$ as

$$\delta\hat{L}_{k,l} = \delta Z_{k-1}\delta_{l,1} + \delta Z_{k-l}(1-\delta_{l,1}), \quad (20)$$

with

$$\delta Z_k = \begin{cases} \frac{\text{u}(E-E_c)}{kQ_c}(-1)^k, & k \neq 0, \\ 0, & k = 0 \end{cases} \quad (21)$$

[compare to Eq. (18)].

Near a critical point $(\text{u}E)_c$ the solution for the Fourier components in Eq. (9) in our linearized approximation can be written in the form

$$\lambda(\text{u}, E) f_k, \quad (22)$$

with the proper permutation of k indices as defined in Eq. (19) and where the coefficient $\lambda(\text{u}, E)$ follows from the solvability condition

$$|\lambda(\text{u}, E)|^2(\text{u}\lambda_1 + \lambda_2) + \sum_{k,k_1} \widetilde{f}_k^*(\delta\hat{L}_{k,k_1}) f_{k_1} = 0, \quad (23a)$$

$$\lambda_3 \text{u}(E - E_c) = \sum_{k,k_1} \tilde{f}_k^*(\delta\hat{L}_{k,k_1}) f_{k_1}; \quad (23b)$$

see Appendix B for explicit expressions for all coefficients λ_i.

The expression for current density then takes the form

$$j = E + |\lambda(\text{u}, E)|^2 \lambda_4 Q \quad (24)$$

(see Appendix B for definition of λ_4).

We note that in the critical region only the coefficient of the zero mode $\lambda(\text{u}, E)$ is dominant and all other coefficients are small, scaling with $|(\text{u}E)_c - \text{u}E|/(\text{u}E)_c$.

Altogether, we can now analyze the critical point in detail. Therefore, we calculate the critical points $\{(\text{u}E)_c, Q_c\}$ numerically for truncated Fourier series with N_k components (indices $k \in \{-N_k/2 + 1, \ldots, N_k/2\}$). These are obtained as simultaneous solutions of the polynomial equations $Q^{N_k}\det(\hat{L}) = 0$ and $Q^{N_k+1}\partial_Q \det(\hat{L}) = 0$ of order $3N_k - 2$ in Q. Figure 4 shows the solutions for $N_k = 24$ (order Q^{70}), where the solid lines represent the solutions of the individual equations. Note that solving the linearized equations for the truncated Fourier series leaves the largest critical values $\{(\text{u}E)_c, Q_c\}$ invariant

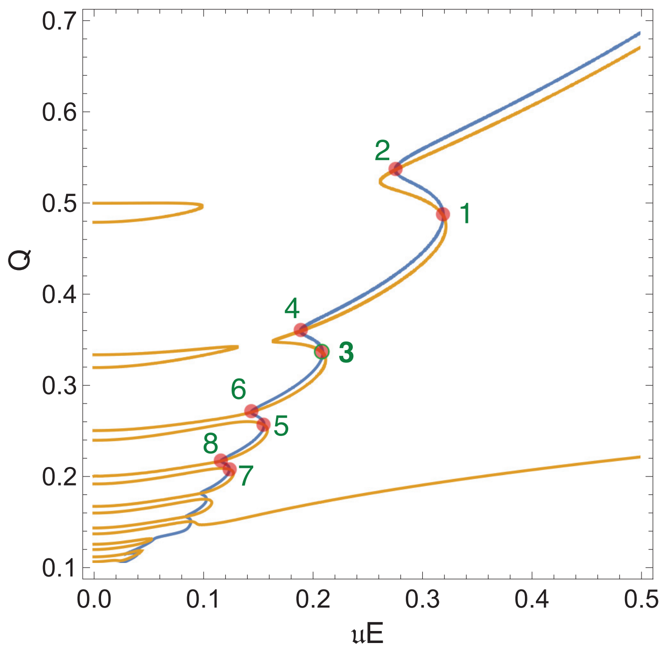

FIG. 4. Solutions of the EV problem for polynomial equations of order Q^{70} and $(\text{u}E)^{24}$ for $N_k = 24$ Fourier components. Depicted are the "zero" lines of the polynomials related to $\det(\hat{L})$ (blue) and $\partial_Q \det(\hat{L})$ (orange) and intersection points corresponding to simultaneous eigenvalue pairs $\{(\text{u}E)_c, Q_c\}$ of $\hat{L}$ and $\hat{L}^\dagger$. The eight largest are marked by circles and labeled.

for sufficiently large N_k. For these solutions we can then obtain the eigenvectors of $\hat{L}$ and $\hat{L}^\dagger$, which allows us then to extract the behavior of the I-V characteristic near these critical points by evaluation of the parameters λ_1, λ_2, and λ_3. At those points new branches appear, which can bring the system out of the normal state. Using Eq. (23b) then defines the slope of the linearized I-V characteristic. The numerical calculation reveals that the critical value $\nu = 3$, $(\text{u}E)_c^{(3)} \approx 0.21$, locally has a negative slope among the eight largest $(\text{u}E)_c$ values, indicating that a reentrance into the superconducting state can happen without a threshold (second order) at a current density j_r. Figure 5 shows the behavior of the order parameter Δ [Fig. 5(a)] and current j [Fig. 5(b)] at the critical points as a function of $\text{u}E$. The connection of the critical points to the envelop (defined by the I-V curve for increasing current) is indicated by dotted lines (these cannot be realized physically). Practically, one can make a hysteresis "loop" in the j-$(\text{u}E)$ diagram by starting in the superconducting state at zero current, following up to j_c upon increasing j, where the system becomes resistive and eventually jumps into to normal state (indicated by an arrow) following the normal I-V curve (blue dashed curve). When decreasing j from the normal state, one follows down the normal I-V line until the critical point labeled $*$ $(\nu = 3)$, where the slope of I-V is negative, such that fluctuating superconducting regions can grow and one jumps back into the superconducting state at j_r (indicated by an arrow). Below this point the normal state is always unstable. At all other (larger) critical points we cannot follow the critical I-V (without a threshold) as the slope is positive (first order). We note that the specific picture depends on the actual value of u for the physical system under consideration; here we assume a value of u of order 1.

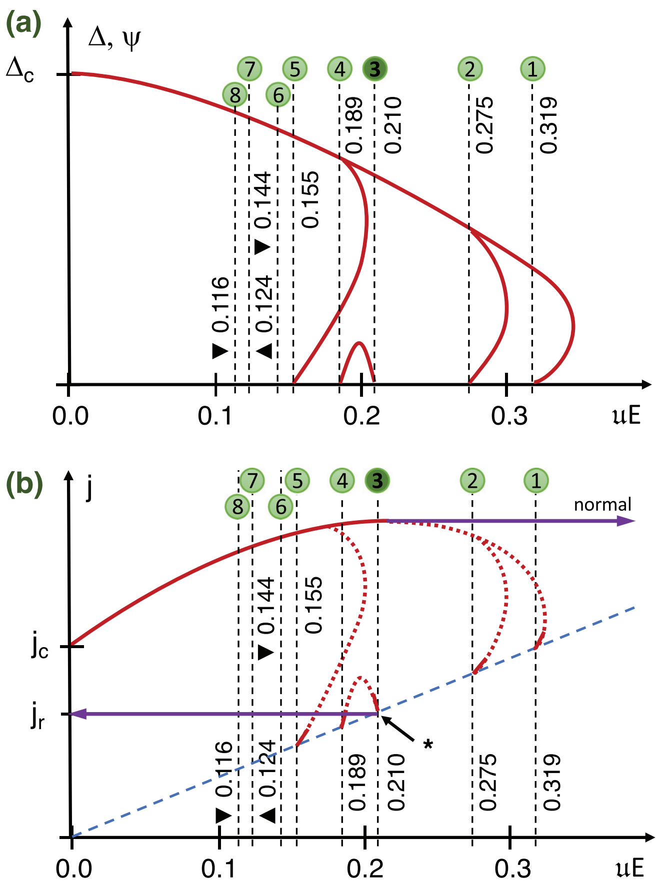

FIG. 5. Critical behavior of the (a) superconducting order parameter and (b) the I-V characteristics, where the eight largest eigenvalues of operators $\hat{L}$ and $\hat{L}^\dagger$ determine the intersection points of the dynamical state and the linear Ohmic behavior, respectively. The critical values should be compared to Fig. 4 and Table I and are indicated by vertical dashed lines and numbered accordingly. The asterisk (∗) indicates the transition to the superconducting state without a threshold for critical value 3. The slope of the I-V curves at the critical points is determined by Eq. (23b), indicated by solid lines. The connection of the critical points to the envelop is indicated by dotted lines (cannot be realized physically). Starting in the superconducting state at zero current, one follows up to j_c upon increasing j, where the system becomes resistive and eventually jumps into to the normal state (indicated by an arrow) following the normal I-V curve (blue dashed curve). When decreasing j from the normal state, one follows down the normal I-V line until the critical point (∗), where the slope of I-V is negative, such that fluctuating superconducting regions can grow, and one jumps back into the superconducting state at j_r (indicated by an arrow). At all other critical points we cannot follow the critical I-V (without a threshold) as the slope is positive.

The numerical analysis demonstrates that probably, an infinite set of solutions of the eigenvalue problem, Eq. (16), exists.

In analogy to finding the (global) extremum of a function on a finite support, where the boundary values also need to be checked, here we should also study the properties of the system close to the hypothetical "end points," if they exist [in addition to the (local) critical points defined by (16)]. By "end points" we mean points of the surface $\{\hat{L}\psi = 0\}$ in Hilbert space, where the value $(\mathrm{u}E)$ reaches its maxima under the condition

$$\sum_{k=2}^{\infty} k|A_k|^2 + |A_1|^2 - \sum_{k=1}^{\infty} k|A_{-k}|^2 = 0. \quad (25)$$

Our numerical evaluation of this condition reveals that such end points are irrelevant.

IV. CONCLUSIONS

We have investigated the I-V characteristic of a superconducting strip in the region near the depairing current j_{dp} and studied the instability points of the normal state as a function of the current. Interestingly, one finds a degeneracy in second-order perturbation theory in the electric field E by solving the linearized equation at those critical points.

This degeneracy leads to the appearance of additional branches splitting off from the Ohmic behavior seen in Fig. 5. Numerically, we calculated the critical points and found that the largest electric field value, at which the normal state first becomes unstable upon decreasing the current, i.e., indicating the possibility of a transition into the superconducting state with a finite value of the order parameter amplitude [see Fig. 5(a)], and a branch in the I-V appears, is at $\mathrm{u}E = 0.3199$. However, the slope of the branch is positive, indicating a first-order transition, which we can follow only when increasing the current (and eventually jumping back in the normal state). Therefore, when increasing the current for fixed $\mathrm{u}E$ in the intervals [0.21,0.275[and]0.275,0.319], a transition into the superconducting state will happen at $\mathrm{u}E = 0.275$ and $\mathrm{u}E = 0.319$, respectively, before returning to the normal state at larger currents. Alternatively, one could do a voltage sweep slightly below these critical points while keeping the current constant to explore the related instability branches. In fact, the latter protocol was used on (NbN and Pb) superconducting nanowires in Refs. [25,26], which further shows the relevance of our results. For the NbN wires it is actually shown that the voltage sweep reveals instability points above the reentrance current (without threshold).

However, most importantly, we also found the smallest value for $\mathrm{u}E$ when the normal state is always unstable to be equal to 0.2095 (indicated by ∗ in Fig. 5), defining the reentrance current into the superconducting state. This hysteretic I-V curve was measured in NbN nanowires in Ref. [26]. In contrast to the evaluation of the critical current, the evaluation of the reentrance current is significantly more involved.

ACKNOWLEDGMENTS

We are delighted to thank I. S. Aranson for interesting discussions. The research was supported by the US Department of Energy, Office of Science, Basic Energy Sciences, Materials Sciences and Engineering Division. Yu.N.O acknowledges Prof. Dr. Jeroen van den Brink for his hospitality in LIFW and the DFG for granting him a Mercator-Professoren-Stipendium. A.A.V. acknowledges financial support from the project CoExAn (HORIZON 2020, Grant Agreement No. 644076) and from the Italian MIUR through the PRIN 2015 program (Contract No. 2015C5SEJJ001).

APPENDIX A: SOLUTION OF TDGLE NEAR THE DEPAIRING CURRENT

Close to the depairing current, Eq. (9) is decomposed into pairwise equations with $\{k, -k+2\}$. For $k \neq 1$

$$\begin{pmatrix} \left[1-2|A_1|^2 - \frac{\mathrm{u}|A_1|^2(k+1)}{2(k-1)} - k^2Q^2\right] & -A_1^2\left(1+\frac{u(3-k)}{2(k-1)}\right) \\ -(A_1^*)^2\left(1-\frac{u(k+1)}{2(k-1)}\right) & \left[1-2|A_1|^2 + \frac{\mathrm{u}|A_1|^2(3-k)}{2(k-1)} - (k-2)^2Q^2\right] \end{pmatrix} \begin{pmatrix} A_k \\ A^*_{-k+2} \end{pmatrix} = \frac{\mathrm{u}E(-1)^k}{(k-1)Q}\begin{pmatrix} -A_1 \\ A_1^* \end{pmatrix}.$$

Solving this system results in

$$A_k = -\frac{1}{\mathcal{D}}\frac{\mathrm{u}E(-1)^kA_1}{(k-1)Q}[1-3|A_1|^2-(k-2)^2Q^2], \quad A^*_{-k+2} = \frac{1}{\mathcal{D}}\frac{\mathrm{u}E(-1)^kA_1^*}{(k-1)Q}[1-3|A_1|^2-k^2Q^2], \tag{A1a}$$

where

$$\mathcal{D} = \left\{1-2|A_1|^2 - [(k-1)^2+1]Q^2 - \frac{\mathrm{u}|A_1|^2}{2}\right\}^2 - \left[2(k-1)Q^2 + \frac{\mathrm{u}|A_1|^2}{k-1}\right]^2 - |A_1|^4\left[\left(1-\frac{\mathrm{u}}{2}\right)^2 - \frac{\mathrm{u}^2}{(k-1)^2}\right]. \tag{A1b}$$

In our approximation, we obtain from Eq. (A1b)

$$\mathcal{D} = \tfrac{1}{9}(k-1)^2[(k-1)^2+2\mathrm{u}] \tag{A2}$$

when the electric field E is much smaller than its critical value E_c.

For $k=1$, we obtain from Eq. (9) the following equation for the quantity $|A_1|^2$ in second-order perturbation theory:

$$\sum_{k=2}^{\infty}\frac{\mathrm{u}}{k-1}\left\{\frac{E(-1)^k}{Q}(A_k - A_{2-k}) - \frac{A_1}{2}[(k+1)|A_k|^2 - (3-k)|A_{k-2}|^2] + (k-1)A_1^*A_kA_{2-k}\right\}$$
$$= A_1(1-|A_1|^2-Q^2) - 2\sum_{k=2}^{\infty}\{A_1(|A_k|^2+|A_{2-k}|^2) + A_1^*A_kA_{2-k}\}. \tag{A3}$$

Using second-order perturbation theory, we can set

$$|A_1| = \sqrt{\frac{2}{3}} + \beta E^2, \quad Q = \frac{1}{\sqrt{3}} + \alpha E^2, \tag{A4}$$

where $\{\alpha, \beta\}$ are constants. Inserting expression (A1a) for the coefficients A_k and expressions (A4) into Eq. (A3), we get the following relation for those constants:

$$\frac{2}{\sqrt{3}}(\alpha + \sqrt{2}\beta) = \sum_{k=2}^{\infty}\left\{\left(\frac{4\mathrm{u}^3}{3\mathcal{D}^2} - \frac{6\mathrm{u}^2}{(k-1)^2\mathcal{D}}\right)\left(1+\frac{(k-1)^2+1}{3}\right) - \frac{4\mathrm{u}^2}{\mathcal{D}^2}\left[\frac{1}{(k-1)^2}\left(1+\frac{(k-1)^2+1}{3}\right)^2 + \frac{4}{3}\right]\right\}. \tag{A5}$$

One important property of Eqs. (A3) and (A4) should be mentioned: in second-order perturbation theory, defined by Eq. (A5), α and β appear only in combination, $\alpha + \sqrt{2}\beta$. This implies that corrections to the quantities $|A_1|$ and Q appear separately in perturbation theory only in order $O(E^4)$

In the same approximation we obtain from Eq. (8)

$$j = \frac{2}{3\sqrt{3}} + E + \frac{2}{3}E^2(\alpha+\sqrt{2}\beta) + \frac{4\mathrm{u}^2E^2}{\sqrt{3}}\sum_{k=0}^{\infty}\frac{1}{(k-1)^2\mathcal{D}^2}\left[\left(1+\frac{(k-1)^2+1}{3}\right)^2 - \frac{4}{3}(k-1)^2 - \frac{4}{9}(k-1)^4\right]. \tag{A6}$$

Inserting Eq. (A5) into expression (A6) yields an expression for the current j in second-order perturbation theory in E:

$$j = \frac{2}{3\sqrt{3}} + E - E^2\gamma(\mathrm{u}), \tag{A7a}$$

$$\gamma(\mathrm{u}) = \frac{2\mathrm{u}^2}{\sqrt{9}}\sum_{k=0}^{\infty}\frac{1}{\mathcal{D}^2}[(k-1)^4 + 12(k-1)^2 + 48]. \tag{A7b}$$

The expression for $\gamma(\mathrm{u})$ in (A7b) can be evaluated explicitly as

$$\gamma(\mathrm{u}) = \frac{\sqrt{3}}{40\mathrm{u}^2}(32\pi^4\mathrm{u}^2 - 30(\mathrm{u}-6)^2 + 15\pi\sqrt{2}[(\mathrm{u}-18)\mathrm{u}+60]\sqrt{\mathrm{u}}\coth(\pi\sqrt{2\mathrm{u}})$$
$$+ 30\pi^2\mathrm{u}\{4(\mathrm{u}-4) + [(\mathrm{u}-6)\mathrm{u}+12]\sinh^{-2}(\pi\sqrt{2\mathrm{u}})\}), \tag{A8}$$

which can be written as the full derivative equation (12).

APPENDIX B: SOLVABILITY AND *I*-*V* AT THE CRITICAL POINTS

The coefficients in the solvability equations, (23a) and (23b), are given by

$$\lambda_1 = \frac{1}{2}\sum_k \widetilde{f}_k^* \left[\sum_{l\neq 0}\frac{1}{l}\left\{[f_1^2(2-l)f_{-l+1}^* + |f_1|^2(2+l)f_{l+1}]\delta_{k,l+1} + \sum_{m\neq 1}[f_1(2-l)f_{-l+1}^* f_m + f_1^*(2+l)f_{l+1}f_m]\delta_{k,l+m}\right\}\right.$$
$$\left. - \frac{1}{2}\sum_{\substack{l,m\neq 1\\ l\neq m}}\frac{l+m}{l-m}\left(f_1 f_l^* f_m \delta_{k,-l+m+1} + \sum_{n\neq 1} f_l^* f_m f_n \delta_{k,m+n-l}\right)\right], \quad \text{(B1a)}$$

$$\lambda_2 = \sum_k \widetilde{f}_k^* \left\{ f_1|f_1|^2\delta_{k,1} + 2|f_1|^2(1-\delta_{k,1})f_k \right.$$
$$\left. + \sum_{l\neq 1}\left[2\sum_{m\neq 1}\left(f_1 f_l f_m^* \delta_{k,l-m+1} + \sum_{n\neq 1} f_l f_m^* f_n \delta_{k,l-m+n}\right) + f_1^2 f_l^* \delta_{k,2-l} + \sum_{m\neq 1} f_1^* f_l f_m \delta_{k,l+m-1}\right]\right\}, \quad \text{(B1b)}$$

$$\lambda_3 = \frac{1}{Q_c}\left[\sum_{k\neq k_1}\frac{(-1)^{k-k_1}}{k-k_1}\widetilde{f}_k^* f_{k_1}\right], \quad \text{(B1c)}$$

$$\lambda_4 = \sum_{k=-\infty}^{\infty} k|f_k|^2. \quad \text{(B1d)}$$

Here $\widetilde{f}_k$ are the components of the normalized eigenvector of the transposed operator $\hat{L}^\dagger = \hat{L}^\mathsf{T}$.
Next, we define the function

$$\Lambda(\mathrm{u}E) \equiv \sum_{k,k_1} \widetilde{f}_k^*(\delta\hat{L}_{k,k_1})f_{k_1} = -|\lambda(\mathrm{u},E)|^2(\mathrm{u}\lambda_1+\lambda_2),$$

where f_k are the components of the eigenvector of $\hat{L}$ and $\widetilde{f}_k$ are the components of the normalized eigenvector of the operator $\hat{L}^\dagger$. The function $\delta\hat{L}_{k,k_1}$ is defined in Eq. (20). Equation (9) in the vicinity of each critical point $\{(\mathrm{u}E)_c, Q_c\}$ can then be rewritten in the form

$$|\lambda(\mathrm{u},E)|^2(\mathrm{u}\lambda_1+\lambda_2) + \lambda_3\mathrm{u}(E-E_c) = 0, \quad \text{(B2)}$$

where the coefficients are given in (B1a)–(B1c). Therefore,

$$|\lambda(\mathrm{u},E)|^2 = -\frac{\Lambda(\mathrm{u}E)}{\mathrm{u}\lambda_1+\lambda_2}.$$

The functions $\Lambda(\mathrm{u}E)$ corresponding to the eight largest critical values $(\mathrm{u}E)_c$ are given by

$$\Lambda^{(1)}(\mathrm{u}E) = 0.0564 - 0.176\mathrm{u}E,$$
$$\Lambda^{(2)}(\mathrm{u}E) = 0.0217 - 0.0787\mathrm{u}E,$$
$$\boldsymbol{\Lambda^{(3)}(\mathrm{u}E) = -0.00629 + 0.03\mathrm{u}E},$$
$$\Lambda^{(4)}(\mathrm{u}E) = 0.00319 - 0.0169\mathrm{u}E,$$
$$\Lambda^{(5)}(\mathrm{u}E) = 0.000888 - 0.00570\mathrm{u}E,$$
$$\Lambda^{(6)}(\mathrm{u}E) = 0.000372 - 0.00258\mathrm{u}E,$$
$$\Lambda^{(7)}(\mathrm{u}E) = 0.000103 - 0.000833\mathrm{u}E,$$
$$\Lambda^{(8)}(\mathrm{u}E) = 0.0000507 - 0.000436\mathrm{u}E.$$

Note the signs of the coefficients in $\Lambda^{(3)}$ at the critical point without threshold (bold). For completeness, we reproduce the corresponding eigenvectors f_k and $\widetilde{f}_k$ in the Supplemental Material [24].

APPENDIX C: DERIVATION OF FOURIER EQUATIONS

Here we will obtain the equation system for the Fourier coefficients A_k. From Eq. (9) we obtain for $k_0 \neq 1$

$$\begin{aligned} &Z_{k_0-1}A_1 + \sum_{k\neq 1} Z_{k_0-k}A_k + \frac{\mathfrak{u}}{2(k_0-1)}[A_1^2(3-k_0)A_{2-k_0}^* + |A_1|^2(k_0+1)A_{k_0}] \\ &+ \sum_{k\notin\{0,k_0-1\}} \frac{\mathfrak{u}}{2k}[A_1(2-k)A_{k_0-k}A_{1-k}^* + (2+k)A_1^*A_{k+1}A_{k_0-k}] \\ &+ \frac{\mathfrak{u}}{2}\sum_{k\neq\{1,2-k_0\}}\left[\frac{2k+k_0-1}{k_0-1}A_1A_k^*A_{k_0+k-1} - \sum_{q\notin\{1,k\}}\frac{k+q}{k-q}A_k^*A_qA_{k_0+k-q}\right] \\ &= \left(1-2|A_1|^2 - Q^2k_0^2\right)A_{k_0} - 2\sum_{k\notin\{1,k_0\}} A_1A_kA_{k-k_0+1}^* \\ &- \sum_{k\neq 1, q\notin\{1,k-K_0+1\}} A_kA_q^*A_{k_0+q-k} - A_1^2A_{2-k_0}^* - A_1^*\sum_{k\notin\{0,k_0\}} A_kA_{k_0-k+1}. \end{aligned} \tag{C1}$$

From Eq. (9) we obtain a separate equation for $k_0 = 1$:

$$\begin{aligned} &\sum_{k\neq 1}\left[Z_{1-k}A_k - \frac{\mathfrak{u}(k+1)}{2(k-1)}(A_1|A_k|^2 - A_1^*A_kA_{2-k}) - \frac{u}{2}\sum_{q\notin\{1,k\}} A_k^*A_qA_{k+1-q}\right] \\ &= A_1(1-|A_1|^2 - Q^2) - \sum_{k\neq 1}\left[2A_1|A_k|^2 + A_1^*A_kA_{2-k} + \sum_{q\notin\{1,k\}} A_kA_q^*A_{1+q-k}\right]. \end{aligned} \tag{C2}$$

Next, we introduce the operator $\hat{M}_{k_0}$ for $k_0 \neq 1$ as

$$\hat{M}_{k_0} = \begin{pmatrix} \left(1-2|A_1|^2 - Q^2k_0^2\right) - \frac{\mathfrak{u}|A_1|^2(k_0+1)}{2(k_0-1)} & -A_1^2\left(1+\frac{\mathfrak{u}(3-k_0)}{2(k_0-1)}\right) \\ -(A_0^*)^2\left(1-\frac{\mathfrak{u}(k_0+1)}{2(k_0-1)}\right) & 1-2|A_1|^2 - Q^2(k_0-2)^2 + \frac{\mathfrak{u}|A_1|^2(3-k_0)}{2(k_0-1)} \end{pmatrix}. \tag{C3}$$

With this, Eq. (1) can be written in the form

$$\hat{M}_{k_0}\begin{pmatrix} A_{k_0} \\ A_{2-k_0}^* \end{pmatrix} = \begin{pmatrix} Z_{k_0-1}A_1 + \sum_{k\neq 1} Z_{k_0-k}A_k \\ Z_{1-k_0}A_1^* + \sum_{k\neq 1} Z_{k-k_0}A_{2-k}^* \end{pmatrix} + \begin{pmatrix} \Phi_{k_0} \\ \Phi_{2-k_0}^* \end{pmatrix}, \tag{C4}$$

where Φ_{k_0} is

$$\begin{aligned} \Phi_{k_0} = &\frac{\mathfrak{u}}{2}\sum_{k\notin\{1,k_0\}}\left[\frac{2k+k_0-1}{k_0-1}A_1A_k^*A_{k_0+k-1} - \sum_{q\notin\{1,k\}}\frac{k+q}{k-q}A_k^*A_qA_{k_0+k-q}\right] \\ &+ \sum_{k\notin\{1,k_0\}}\frac{k}{2(k-1)}[A_2(3-k)A_{2-k}^* + A_2^*(1+k)A_k]A_{k_0-k+1} \\ &+2\sum_{k\notin\{1,k_0\}} A_1A_kA_{k-k_0+1}^* + \sum_{k\neq 1, q\notin\{1,k-k_0+1\}} A_kA_q^*A_{k_0+q-k} + A_1^*\sum_{k\notin\{0,k_0\}} A_kA_{k_0-k+1}. \end{aligned} \tag{C5}$$

Note that a free parameter Q appears in Eqs. (C2) and (C4). The value of this parameter is found with the extremal condition for the electric field E for a given current density j.

[1] M. Sahu, M.-H. Bae, A. Rogachev, D. Pekker, T.-C. Wei, N. Shah, P. M. Goldbart, and A. Bezryadin, Nat. Phys. **5**, 503 (2009).
[2] A. Bezryadin, *Superconductivity in Nanowires: Fabrication and Quantum Transport* (Wiley-VCH Verlag GmbH & Co. KGaA, Weinheim, Germany, 2012).
[3] J. S. Langer and V. Ambegaokar, Phys. Rev. **164**, 498 (1967).
[4] M. Tinkham, *Introduction to Superconductivity* (McGraw-Hill Inc., New York, 1996).
[5] W. J. Skocpol, M. R. Beasley, and M. Tinkham, J. Low. Temp. Phys. **16**, 145 (1974).
[6] L. Kramer and A. Baratoff, Phys. Rev. Lett. **38**, 518 (1977).
[7] L. Kramer and R. Rangel, J. Low. Temp. Phys. **57**, 391 (1984).
[8] R. Rangel and L. Kramer, J. Low. Temp. Phys. **74**, 163 (1989).

[9] C. N. Lau, N. Markovic, M. Bockrath, A. Bezryadin, and M. Tinkham, Phys. Rev. Lett. **87**, 217003 (2001).

[10] J. Mooij and Y. V. Nazarov, Nat. Phys. **2**, 169 (2006).

[11] D. McKay, M. White, M. Pasienski, and B. DeMarco, Nature (London) **453**, 76 (2008).

[12] G. Kimmel, A. Glatz, and I. S. Aranson, Phys. Rev. B **95**, 014518 (2017).

[13] A. Glatz and T. Nattermann, Phys. Rev. Lett. **88**, 256401 (2002).

[14] P. Scherpelz, K. Padavić, A. Rançon, A. Glatz, I. S. Aranson, and K. Levin, Phys. Rev. Lett. **113**, 125301 (2014).

[15] P. Scherpelz, K. Padavić, A. Murray, A. Glatz, I. S. Aranson, and K. Levin, Phys. Rev. A **91**, 033621 (2015).

[16] Note that material defects and weak links also lead to phase-slip events [12,27–29], but here we concentrate on the clean case.

[17] Y. N. Ovchinnikov and A. A. Varlamov, Phys. Rev. B **91**, 014514 (2015).

[18] B. Ivlev and N. Kopnin, Adv. Phys. **33**, 47 (1984).

[19] N. B. Kopnin and B. I. Ivlev, Sov. Phys. Usp. **27**, 206 (1984).

[20] L. P. Gorkov, JETP Lett. **11**, 32 (1970).

[21] I. O. Kulik, Zh. Eksp. Teor. Fiz. **59**, 584 (1971) [Sov. Phys. JETP **32**, 318 (1971)].

[22] Y. N. Ovchinnikov, J. Exp. Theor. Phys. **85**, 818 (1997).

[23] N. Kopnin, *Theory of Nonequilibrium Superconductivity*, International Series of Monographs on Physics (Oxford University Press, Oxford, 2001).

[24] See Supplemental Material at http://link.aps.org/supplemental/10.1103/PhysRevB.101.014511 for a full list of the eight largest eigenvalues and eigenvectors near critical points.

[25] D. Y. Vodolazov, F. M. Peeters, L. Piraux, S. Mátéfi-Tempfli, and S. Michotte, Phys. Rev. Lett. **91**, 157001 (2003).

[26] A. K. Elmurodov, F. M. Peeters, D. Y. Vodolazov, S. Michotte, S. Adam, F. de Menten de Horne, L. Piraux, D. Lucot, and D. Mailly, Phys. Rev. B **78**, 214519 (2008).

[27] L. Kramer and R. J. Watts-Tobin, Phys. Rev. Lett. **40**, 1041 (1978).

[28] R. J. Watts-Tobin, Y. Krähenbühl, and L. Kramer, J. Low Temp. Phys. **42**, 459 (1981).

[29] G. Berdiyorov, K. Harrabi, F. Oktasendra, K. Gasmi, A. I. Mansour, J. P. Maneval, and F. M. Peeters, Phys. Rev. B **90**, 054506 (2014).